On Estimating Time-Varying Pauli Noise

Junaid ur Rehman, Hayder Al-Hraishawi, *Senior Member, IEEE*, Trung Q. Duong, *Fellow, IEEE*, Symeon Chatzinotas, *Fellow, IEEE*, and Hyundong Shin, *Fellow, IEEE*

***Abstract*—We consider the problem of estimating time-varying quantum noise. Specifically, we focus on Pauli qubit noise with time-variations and attempt to construct the most accurate instantaneous channel description. To this end, we propose an adaptive framework of simultaneous communication and parameter estimation (SCAPE) that efficiently and accurately estimates the time-varying Pauli channel while communicating reliably over the channel being estimated. This adaptive framework gives the informed control of communication rate–parameter estimation tradeoff to communicating parties. Interestingly, this adaptive SCAPE requires post-processing entirely on the receiver's end and minimal feedback to the sender to increase, decrease, or continue with the same code rate of employed error correcting code. This procedure can be particularly useful in time-varying quantum channels with natural periodic deviations in channel conditions, e.g., in satellite communication channels.**

***Index Terms*—Adaptive coding and modulation, diamond-norm distance, Pauli channels, quantum noise, time-varying noise.**

I. Introduction

RECENT advances in quantum information technologies has brought quantum devices that are larger than a few qubits in size. Despite their intermediate size, noise in these devices limit the size of circuits that can be executed reliably [1]. This limitation can be circumvented by making progress in quantum hardware design to obtain low noise qubits [2]–[4] as well as by designing appropriate countermeasures such as efficient quantum error correcting codes and quantum error mitigation methods [5], [6]. Accurate identification and characterization of noise is an important task to design appropriate countermeasures that lead to efficient utilization of these noisy intermediate-scale quantum (NISQ)-era systems [7]–[10].

Traditionally, system identification and utilization are considered fundamentally and operationally separate tasks. However, there have been recent efforts to utilize the available system into the identification stage, bridging the gap between these two processes [11]–[14]. For example, [11] introduced a method that leverages redundancies in quantum error correction codes to estimate bit flip and phase flip errors during quantum information processing. In [12], authors utilized online Gaussian process to estimate the error rates from syndrome measurements [15]. Recently, authors of [13] derived a general condition for the identifiability of the error rates. Under the assumption of sufficiently small error rates, they proved the identifiability for general stabilizer codes. In another related work [14], it was shown that Pauli channel parameters can be estimated from syndrome measurements in quantum error correction. These aforementioned works completely/partially estimate the noisy channel while the system is being utilized for general quantum information processing. They do so by exploiting the redundancy introduced by the quantum error correction codes. A recent work by some of the authors proposed simultaneous communication and parameter estimation (SCAPE) of Pauli channels based on classical error correction codes [16]. These proposals, and quantum process tomography in general, assume quantum channels to be time-independent, i.e., noise levels in quantum circuit or quantum communication channel remain constant.

Indeed, if parameters of a quantum channel are constant or do not vary significantly over time such that the employed error correcting code (ECC) remains sufficient, SCAPE and other protocols described above can be utilized for quantum channel tracking over time. However, recent experiments have shown that physical quantum noise in quantum computing devices may exhibit significant time-variations due to fluctuations in control circuitry or changing environmental conditions [17]–[19]. Similar observations can be made about satellite channels due to time-variations of background radiations through different times of day and different seasons [20]. If these variations in the channel are significant, these methods of simultaneous identification and utilization of quantum channels will fail (resp. be inefficient) due to the failure (resp. low code rates) of employed ECC. Efforts are already underway to characterize these time-variations in quantum noise and devise efficient techniques to mitigate the resulting errors [19], [21], [22].

In this work, we consider the problem of estimating time-varying Pauli channels. In this context, joint system identification and utilization appears to be the most natural strategy to keep up-to-date description of underlying channel at all times. The main contribution of this work is the proposal of adaptive SCAPE framework that avoids the silent failure of the employed ECC. This framework is capable of dynamically adjusting the code rate of employed error correcting codes and the number of samples considered in channel estimation, effectively tailoring these parameters to suit the prevailing

J. ur Rehman, H. Al-Hraishawi, and S. Chatzinotas are with the the Interdisciplinary Centre for Security, Reliability, and Trust (SnT), Luxembourg, L-1855 Luxembourg (e-mail: junaid.urrehman@uni.lu). Trung Q. Duong is with the Faculty of Engineering and Applied Science, Memorial University of Newfoundland, St. John's, NL A1C 5S7, Canada, and also with the School of Electronics, Electrical Engineering and Computer Science, Queen's University Belfast, BT7 1NN Belfast, U.K. (e-mail: tduong@mun.ca). H. Shin is with the Department of Electronics and Information Convergence Engineering, Kyung Hee University, 1732 Deongyeong-daero, Giheung-gu, Yongin-si, Gyeonggi-do 17104 Korea (email: hshin@khu.ac.kr)

The work of T. Q. Duong was supported in part by the Canada Excellence Research Chair program. The work of H. Shin was supported by the National Research Foundation of Korea (NRF) grant funded by the Korean government (MSIT) (NRF-2019R1A2C2007037, NRF-2022R1A4A3033401) and by the MSIT (Ministry of Science and ICT), Korea, under the ITRC (Information Technology Research Center) support program (IITP-2023-2021-0-02046) supervised by the IITP (Institute for Information & Communications Technology Planning & Evaluation). *(Corresponding author: Hyundong Shin.)*

TABLE I
A SUMMARY OF EIGENBASES OF PAULI QUBIT OPERATORS AND THEIR EVOLUTION UNDER THE ACTION OF PAULI OPERATORS.

Operator, Eigenbasis	Operation on Pauli Operators' Eigenbasis
X (Hadamard basis) $\mathcal{B}_X = \{\|0_X\rangle, \|1_X\rangle\}$ $\|0_X\rangle = \begin{bmatrix}1/\sqrt{2} & 1/\sqrt{2}\end{bmatrix}^\top$ $\|1_X\rangle = \begin{bmatrix}1/\sqrt{2} & -1/\sqrt{2}\end{bmatrix}^\top$	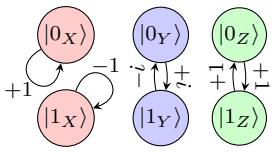
Y $\mathcal{B}_Y = \{\|0_Y\rangle, \|1_Y\rangle\}$ $\|0_Y\rangle = \begin{bmatrix}1/\sqrt{2} & \imath/\sqrt{2}\end{bmatrix}^\top$ $\|1_Y\rangle = \begin{bmatrix}1/\sqrt{2} & -\imath/\sqrt{2}\end{bmatrix}^\top$	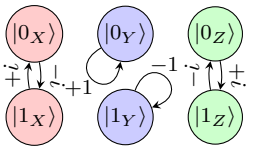
Z (Computational basis) $\mathcal{B}_Z = \{\|0_Z\rangle, \|1_Z\rangle\}$ $\|0_Z\rangle = \begin{bmatrix}1 & 0\end{bmatrix}^\top$ $\|1_Z\rangle = \begin{bmatrix}0 & 1\end{bmatrix}^\top$	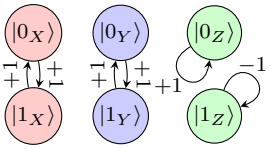

channel conditions. A summary of specific contributions of this manuscript is as follows:

- We introduce the codeword reliability index (CRI) for repetition codes that allows the receiver to independently assess the reliability of received codewords. This CRI serves the crucial role of assessing both communication and estimation reliability of adaptive SCAPE. The feedback value of changing the code rates at the transmitter end are based on the minimum CRI values encountered in each Pauli basis over Pauli channel. A complete system diagram of adaptive SCAPE is shown in Fig. 1.
- We demonstrate that increasing the number of samples in estimation to achieve more accurate estimates is no longer true in time-varying channels due to multiple factors. Through numerical examples we show that the average error in time-varying channels estimates is convex in the number of samples. Despite being convex, it is not possible to minimize it in practical settings due to unavailability of ground-truth knowledge of channel. We introduce average inter-estimate distance as a de facto objective function that can be minimized to obtain the value of near-optimal number of samples to minimize the estimation error. The average inter-estimate distance can be readily estimated from already obtained channel estimates and does not require ground-truth description of quantum channel.
- We present simulations results to showcase the validity and effectiveness of proposed framework for estimating time-varying Pauli channels. Through extensive numerical examples, we demonstrate the improved performance of adaptive SCAPE over entanglement-free parameter estimation (EFPE) and regular SCAPE introduced in [16]. For communication, specific advantage over EFPE is the utilization of all channel time for communication without dedicating specific time-frames for estimation. In comparison to regular SCAPE, communication improvements include i) clear indicators of failing ECC, ii) adaptive code rates, and iii) consequently smaller bit error rates. For estimation, the improvement over EFPE is the availability of always up-to-date and precise channel knowledge. In comparison to regular SCAPE, adaptive SCAPE provides accurate channel estimates even in high-noise regime with clear indicators if the obtained channel estimates as well as the communicated message might be unreliable.

The developments in this manuscript utilize the non-adaptive SCAPE protocol of [16] as a core element while developing necessary mathematical tools to adapt the coding rate to the channel conditions. Without these developments, the non-adaptive SCAPE protocol fails to perform if the noise level in the channel varies significantly from the initially expected noise level. We discuss this point in detail in Section III and Subsection IV-A.

The remainder of this paper is organized as follows. In Section II, we introduce preliminaries, set some notation, and describe the EFPE scheme of [23]. We briefly review the SCAPE protocol of [16] in Section III. We develop the adaptive SCAPE protocol in Section IV and provide numerical examples. We finally conclude our discussion and provide future outlook in Section V.

II. PRELIMINARIES

A. Notation

A quantum state is represented by a density operator ρ, which is a Hermitian operator with unit trace on the Hilbert space $\mathcal{H}$. When the state ρ is pure, i.e., $\rho = |\psi\rangle\langle\psi|$, where $|\psi\rangle \in \mathcal{H}$, we utilize the shorthand notation of denoting the state by $|\psi\rangle$.

We dedicate $\mathcal{N}$ to denote an arbitrary quantum channel, possibly with a subscript if required. In this work, we focus on the Pauli qubit channel, defined as

$$\mathcal{N}_{\mathrm{PQ}}(\rho) = p_I\rho + p_X X\rho X^\dagger + p_Y Y\rho Y^\dagger + p_Z Z\rho Z^\dagger, \quad (1)$$

where $(\cdot)^\dagger$ denotes the conjugate transpose of a matrix, $\boldsymbol{p} = [p_I, p_X, p_Y, p_Z]^\top$ forms a probability vector, and

$$X = \begin{bmatrix}0 & 1\\ 1 & 0\end{bmatrix}, Y = \begin{bmatrix}0 & -\iota\\ \iota & 0\end{bmatrix}, \text{ and } Z = \begin{bmatrix}1 & 0\\ 0 & -1\end{bmatrix} \quad (2)$$

with $\iota = \sqrt{-1}$ are the Pauli matrices. We denote, by $\mathcal{B}_X, \mathcal{B}_Y$, and $\mathcal{B}_Z$ the eigenbases of Pauli X, Pauli Y, and Pauli Z operators, respectively. A summary of these eigenbases and their evolution under Pauli operators is shown in Table I. Estimation of a Pauli channel means estimation of $\boldsymbol{p}$ for a physically available but unknown Pauli channel. The estimator of a quantity x is denoted by $\hat{x}$.

B. Pauli Channels Simulating Binary Symmetric Channels

We make repeated use of the fact that a Pauli qubit channels act as binary symmetric channels when the inputs to the channel are eigenstates of one of the Pauli operators and the output of the channel is measured in the eigenbasis of the same Pauli operator [24]. This fact is a consequence of the simple

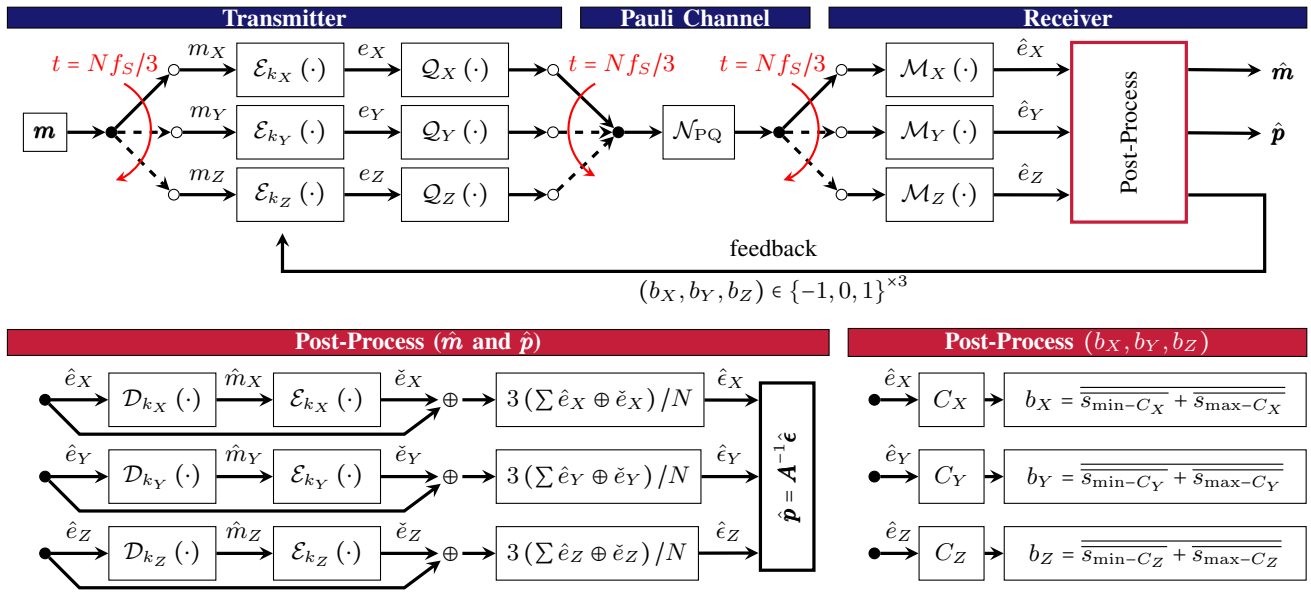

Fig. 1. Adaptive SCAPE protocol with feedback block. $\mathcal{Q}_X$, $\mathcal{Q}_Y$, and $\mathcal{Q}_Z$ are bit-to-qubit encoding blocks in $\mathcal{B}_X$, $\mathcal{B}_Y$, and $\mathcal{B}_Z$, respectively. Similarly, $\mathcal{M}_X$, $\mathcal{M}_Y$, and $\mathcal{M}_Z$ are measurements in $\mathcal{B}_X$, $\mathcal{B}_Y$, and $\mathcal{B}_Z$, respectively. In addition to obtaining $\hat{\boldsymbol{m}}$ and $\hat{\boldsymbol{p}}$, the receiver calculates the CRI of every codeword received in each basis. The overline $\bar{\cdot}$ denotes the $\operatorname{sgn}(\cdot)$ function, which returns $+1$, -1 and 0, for positive numbers, negative numbers and zero, respectively. The feedback b_X, b_Y, and b_Z are calculated based on the lowest value of CRI encountered in each basis.

observation that Pauli operators act as NOT operator on the eigenstates of other Pauli operators as shown in Table I.

Example 1: Let the input to a Pauli qubit channel be from the set $\mathcal{B}_X = \{|0_X\rangle, |1_X\rangle\}$. Then,

$$\mathcal{N}_{\mathrm{PQ}}(|0_X\rangle\langle 0_X|) = (p_I + p_X)|0_X\rangle\langle 0_X| + (p_Y + p_Z)|1_X\rangle\langle 1_X|, \tag{3}$$

and

$$\mathcal{N}_{\mathrm{PQ}}(|1_X\rangle\langle 1_X|) = (p_I + p_X)|1_X\rangle\langle 1_X| + (p_Y + p_Z)|0_X\rangle\langle 0_X|. \tag{4}$$

This gives the crossover probability

$$\begin{aligned}\mathbb{P}\{|0_X\rangle \mid |1_X\rangle\} &= \operatorname{tr}(\mathcal{N}_{\mathrm{PQ}}(|1_X\rangle\langle 1_X|)|0_X\rangle\langle 0_X|) \\ &= \operatorname{tr}(\langle 0_X|\mathcal{N}_{\mathrm{PQ}}(|1_X\rangle\langle 1_X|)|0_X\rangle) \\ &\overset{(a)}{=} p_Y + p_Z \equiv \epsilon_X,\end{aligned} \tag{5}$$

where (a) follows from substituting the expression of $\mathcal{N}_{\mathrm{PQ}}(|1_X\rangle\langle 1_X|)$ from above and then utilizing the orthonormality of eigenbasis of unitary operator X. It is simple to verify that $\mathbb{P}\{|1_X\rangle \mid |0_X\rangle\} = \mathbb{P}\{|0_X\rangle \mid |1_X\rangle\} = \epsilon_X$. The probability of correct transmission can be similarly calculated as

$$\mathbb{P}\{|0_X\rangle \mid |0_X\rangle\} = \mathbb{P}\{|1_X\rangle \mid |1_X\rangle\} = p_I + p_X = 1 - \epsilon_X, \tag{6}$$

where the last equality follows since $\boldsymbol{p}$ is a probability vector. These probabilities verify that the Pauli qubit channel indeed acts as a binary symmetric channel with the crossover probability ϵ_X in this setting. We denote the simulated binary symmetric channel in this setting as $\mathrm{BSC}_X(\epsilon_X)$.

C. Estimation of Pauli Channels

This subsection briefly explains the entanglement-free parameter estimation (EFPE) protocol for Pauli channels. Following the same procedure as Example 1, we can obtain two more binary symmetric channels $\mathrm{BSC}_Y(\epsilon_Y)$ and $\mathrm{BSC}_Z(\epsilon_Z)$ with crossover probabilities $\epsilon_Y = p_X + p_Z$ and $\epsilon_Z = p_X + p_Y$ by choosing the signal states (and measurements) from $\mathcal{B}_Y$ and $\mathcal{B}_Z$, respectively. We can write the following matrix equality that gives the relation between $\boldsymbol{p}$ that defines the Pauli qubit channel and crossover probabilities

$$\begin{bmatrix} 0 & 0 & 1 & 1 \\ 0 & 1 & 0 & 1 \\ 0 & 1 & 1 & 0 \\ 1 & 1 & 1 & 1 \end{bmatrix} \begin{bmatrix} p_I \\ p_X \\ p_Y \\ p_Z \end{bmatrix} = \begin{bmatrix} \epsilon_X \\ \epsilon_Y \\ \epsilon_Z \\ 1 \end{bmatrix}, \tag{7}$$

where the last row captures the fact that $\boldsymbol{p}$ is a probability vector whose entries sum to unity. We simply write this equality as $\boldsymbol{A}\boldsymbol{p} = \boldsymbol{\epsilon}$. Considering this matrix equality, we can make a simple protocol for Pauli channel estimation. Given N accesses to an unknown Pauli channel, we can obtain $\hat{\boldsymbol{p}}$ as follows [23]. Input $|0_X\rangle$, $|0_Y\rangle$, and $|0_Z\rangle$ to the Pauli channel $N/3$ number of times each. By measuring the corresponding channel outputs in $\mathcal{B}_X$, $\mathcal{B}_Y$, and $\mathcal{B}_Z$, respectively, we can obtain $\hat{\epsilon}_X$, $\hat{\epsilon}_Y$, and $\hat{\epsilon}_Z$. Finally, $\hat{\boldsymbol{p}}$ can be obtained by

$$\hat{\boldsymbol{p}} = \boldsymbol{A}^{-1}\hat{\boldsymbol{\epsilon}}$$
$$\begin{bmatrix} \hat{p}_I \\ \hat{p}_X \\ \hat{p}_Y \\ \hat{p}_Z \end{bmatrix} = \begin{bmatrix} -1/2 & -1/2 & -1/2 & 1 \\ -1/2 & 1/2 & 1/2 & 0 \\ 1/2 & -1/2 & 1/2 & 0 \\ 1/2 & 1/2 & -1/2 & 0 \end{bmatrix} \begin{bmatrix} \hat{\epsilon}_X \\ \hat{\epsilon}_Y \\ \hat{\epsilon}_Z \\ 1 \end{bmatrix}. \tag{8}$$

This is known as the EFPE protocol for Pauli channel estimation introduced in [23] for $d = 2$, i.e., for qubits.

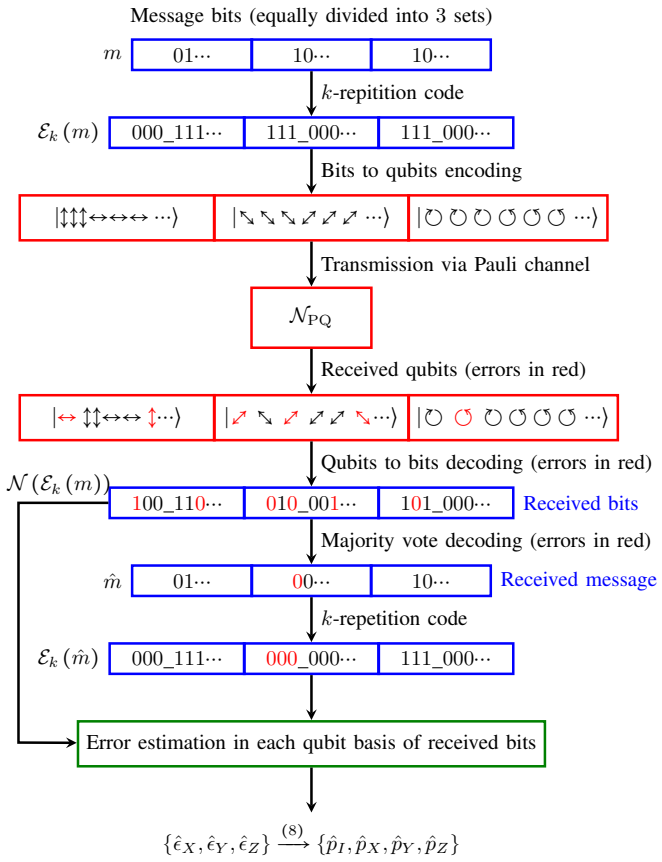

Fig. 2. A visual representation of SCAPE protocol of [16]. Channel statistics can be obtained reliably if the ECC is strong enough.

For numerical examples, we generate the parameters of Pauli channels from the ordered eigenvalues of 4-dimensional normalized correlation matrix [25]

$$\mathbf{\Phi}(\gamma) = \frac{1}{4}\begin{bmatrix} 1 & \gamma & \gamma^2 & \gamma^3 \\ \gamma & 1 & \gamma & \gamma^2 \\ \gamma^2 & \gamma & 1 & \gamma \\ \gamma^3 & \gamma^2 & \gamma & 1 \end{bmatrix}. \tag{9}$$

By varying γ from 0 to 1, we obtain a smooth transition from the maximally noisy (completely depolarizing) channel to the noiseless one.

We quantify the performance of the parameter estimation by the diamond norm distance between the actual and the estimated channel [26], [27]. The diamond norm distance between two different Pauli channels $\mathcal{N}_{\mathrm{PQ}}(\rho) = p_I\rho + p_X X\rho X^\dagger + p_Y Y\rho Y^\dagger + p_Z Z\rho Z^\dagger$ and $\mathcal{M}_{\mathrm{PQ}}(\rho) = q_I\rho + q_X X\rho X^\dagger + q_Y Y\rho Y^\dagger + q_Z Z\rho Z^\dagger$ is given by the sum of the absolute difference between the channel parameters [28], [29], i.e.,

$$\|\mathcal{N}_{\mathrm{PQ}} - \mathcal{M}_{\mathrm{PQ}}\|_\diamond = \sum_{i\in\{I,X,Y,Z\}} |p_i - q_i|. \tag{10}$$

The estimation performance can be benchmarked by computing the diamond norm distance between the estimated channel $\hat{\mathcal{N}}_{\mathrm{PQ}}$ and the actual channel $\mathcal{N}_{\mathrm{PQ}}$, i.e.,

$$\left\|\mathcal{N}_{\mathrm{PQ}} - \hat{\mathcal{N}}_{\mathrm{PQ}}\right\|_\diamond = \sum_{i\in\{I,X,Y,Z\}} |p_i - \hat{p}_i|. \tag{11}$$

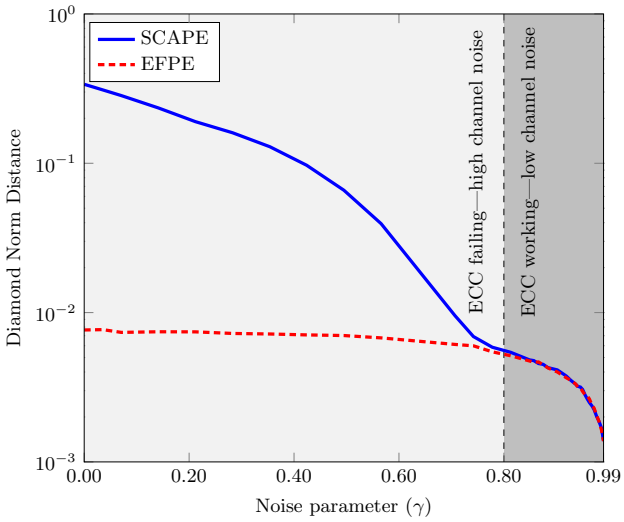

Fig. 3. A comparison of SCAPE (with $k = 13$) and EFPE for different noise strengths. The performance of SCAPE differs significantly from EFPE when the ECC fails due to high channel noise. The plotted curves are the average of $M = 10^3$ simulations with $N = 10^5$ channel uses each.

The communication performance is characterized by the communication rate (bits/channel use), which is simply $1/k$ for the repetition codes. Second performance metric for the communication is the bit error rate of the message.

III. Simultaneous Communication and Parameter Estimation of Pauli Channels

In the estimation scheme of Pauli channels, the knowledge of channel input is crucial for estimation. For this reason, the input to $\mathrm{BSC}_X(\epsilon_X)$ is fixed to $|0_X\rangle$. Without fixing the input to a single state, or to a predetermined sequence agreed between the transmitter and the receiver, it is not possible for the receiver to estimate the number of bit flips and hence ϵ_X. It was shown in [16] that it is possible to utilize *classical* ECC to achieve SCAPE of Pauli channels.

The basic idea of [16] is that it is possible to identify channel errors if the employed ECC is able to sufficiently protect the message from channel errors. More concretely, let m be the message to be transmitted and let $\mathcal{E}_k(\cdot)$ and $\mathcal{D}_k(\cdot)$ be the encoder and decoder operations for some ECC $\mathcal{C}_k$, with some identifier k.[1] The decoded message at the receiver end is $\hat{m} = \mathcal{D}_k(\mathcal{N}(\mathcal{E}_k(m)))$. The comparison of received encoded message $\mathcal{N}(\mathcal{E}_k(m))$ and the encoded received message $\mathcal{E}_k(\hat{m})$ reveals the channel errors, if $m \approx \hat{m}$. We term this as *decode-and-encode* strategy. Thus, if the ECC is strong enough, the receiver can reliably receive the transmitted message as well as generate an estimate of the number of channel errors. Applying this idea for $\mathrm{BSC}_X(\cdot)$, $\mathrm{BSC}_Y(\cdot)$, and $\mathrm{BSC}_Z(\cdot)$, remote parties can simultaneously communicate and estimate the parameters of Pauli channel by employing (8). Specific steps of this protocol are visually illustrated in Fig. 2 and detailed below.

[1] We will utilize k-repetition codes.

Protocol 1: Simultaneous communication and parameter estimation (SCAPE) Protocol [16]

Communicating Parties: Alice: transmitter, Bob: receiver.

Variables:
- $k \geq 3$: number of symbol repetitions, agreed between Alice and Bob.
- N: Total number of channel uses allowed. Assumed to be divisible by $3k$ for simplicity.
- m: message to be sent. Assumed to be of length N/k for simplicity. Divided into equal portions m_X, m_Y, and m_Z.

Protocol steps are as follows:

1. for $j \in \{X, Y, Z\}$, Alice and Bob repeat the following steps:
   - **a.** Alice picks m_j as the message to be transmitted.
   - **b.** Alice computes the k-repetition encoded message $E_j^k = \mathcal{E}_k(m_j)$.
   - **c.** Alice modulates classical bits E_j^k onto qubits using the following mapping
   $$0 \to |0_j\rangle, \quad 1 \to |1_j\rangle.$$
   Let $|\psi_j\rangle$ denote the resulting string of $N/3$ qubits.
   - **d.** Alice sends $|\psi_j\rangle$ to Bob through $N/3$ uses of quantum channel $\mathcal{N}$.
   - **e.** Bob receives $\rho_j = \mathcal{N}(|\psi_j\rangle\langle\psi_j|)$.
   - **f.** Bob measures ρ_j in Pauli j basis to obtain classical estimate $\hat{E}_j^k$ of E_j^k.
   - **g.** Bob decodes $\hat{E}_j^k$ by majority vote decoding to obtain the estimate $\hat{m}_j = \mathcal{D}_k\left(\hat{E}_j^k\right)$ of transmitted message m_j. This completes the message transmission part.
   - **h.** Bob re-encodes $\hat{m}_j$ by k-repetition code to obtain $\hat{E}_j^k = \mathcal{E}_k(\hat{m}_j)$
   - **i.** Bob estimates the channel error rate by
   $$\hat{\epsilon}_j = \frac{3}{N}\sum_{\ell=1}^{N/3} I\left(\check{E}_j^k(\ell), \hat{E}_j^k(\ell)\right),$$
   where $\hat{E}_j^k(\ell)$ is the ℓth bit of $\hat{E}_j^k$ and $I(a,b)$ is the indicator function that is equal to one if $a \neq b$ and zero otherwise.
2. Bob uses (8) with the estimated channel error rates $\hat{\epsilon}_X$, $\hat{\epsilon}_Y$, and $\hat{\epsilon}_Z$ to obtain $\hat{p}_I$, $\hat{p}_X$, $\hat{p}_Y$, and $\hat{p}_Z$, which completes the Pauli channel estimation.

In the case of ECC not being strong enough, this decode-and-encode strategy will *underestimate* the channel noise. To see this, imagine a two-bit error in the codeword of 3-repetition code. The decode-and-encode strategy will miscorrect it to the complementary codeword and will estimate there to be only a single error. Even worse, the receiver cannot identify such events and thus is unable to assess the performance of simultaneous communication and parameter estimation of quantum channels. In such cases, not only the communicated message has high error rate but also the performance of parameter estimation part is affected. Fig. 3 shows the performance comparison of SCAPE with $k = 13$ and EFPE.

IV. SCAPE for Time-Varying Pauli Channels

In this section, we discuss the application of SCAPE protocol for time-varying Pauli channels. As discussed earlier, direct application of SCAPE for time-varying channels may lead to the poor communication and estimation performance if the channel becomes too noisy to be handled by the employed ECC.

One possible solution to avoid this failure of SCAPE is to assume the pessimistic values of noise and use very small code rates. However, this approach will make SCAPE inefficient in term of communication. Further, in an event of degradation of channel beyond anticipated worst-case will lead to the failure of both communication and estimation modules, without the knowledge of communicating parties. Another possible approach is to estimate the channel in one time-step using EFPE and use this channel knowledge for communication in the next time-step. This approach leads to a high overhead since it leads to the wastage of at least half of the available time from communications perspective.

In the upcoming text, we numerically demonstrate these points. In order to simulate a time-varying Pauli channel, we vary the correlation coefficient γ in (9) according to the following sinusoid

$$\gamma(t) = b + a\sin(2\pi f t + \phi), \tag{12}$$

where a is the amplitude of variation, b is the bias, f is the frequency of channel variation, and t is the time. We generate the channel

$$\begin{aligned}\mathcal{N}_{\mathrm{PQ}}(\rho, t) = \lambda_0(t)\rho + \lambda_1(t) X\rho X^\dagger + \\ \lambda_2(t) Y\rho Y^\dagger + \lambda_3(t) Z\rho Z^\dagger,\end{aligned} \tag{13}$$

where $\lambda_i(t)$ are time-varying eigenvalues of (9) in descending order ($\lambda_0(t) \geq \lambda_1(t) \geq \lambda_2(t) \geq \lambda_3(t)$). The signaling/sampling rate is assumed to be f_S, i.e., f_S states can be input and measured at the output of the channel in a second to collect f_S samples. Each estimation step is based on N independent, but not identically distributed, samples collected from the channel.

Fig. 4 illustrates the performance of Pauli channel estimation with SCAPE ($k = 5$) and EFPE. We observe that EFPE with alternative steps of estimation and communication performs better than SCAPE with $k = 5$. However, this better estimation performance comes at the cost of fewer communicated bits. Nevertheless, the performance of both SCAPE and EFPE on time-varying channels is worse than the performance of EFPE on time-invariant channels. There are two sources of errors in this poor performance. In the following, we discuss these sources of errors and strategies to mitigate these errors.

A. Failure of ECC

The first source of error has been highlighted earlier and is unique to SCAPE, i.e., the failure of employed ECC that leads to underestimating the noise strength. This can be seen in high-noise regime of Fig. 4(b), i.e., during $0.3 \leq t \leq 0.7$ and $1.3 \leq t \leq 1.7$ where p_I values are estimated to be higher than the actual values.

In order to circumvent this, we propose the following strategy to adapt the coding rate to the channel condition inferred by the measurement statistics. In a k-repetition code, the receiver performs the majority vote decoding. The codeword is decoded to bit 0 if the number of zeros N_0 is greater than the number of ones N_1. Otherwise it is decoded as bit 1. Thus, a codeword is decoded correctly iff the number of corrupted bits

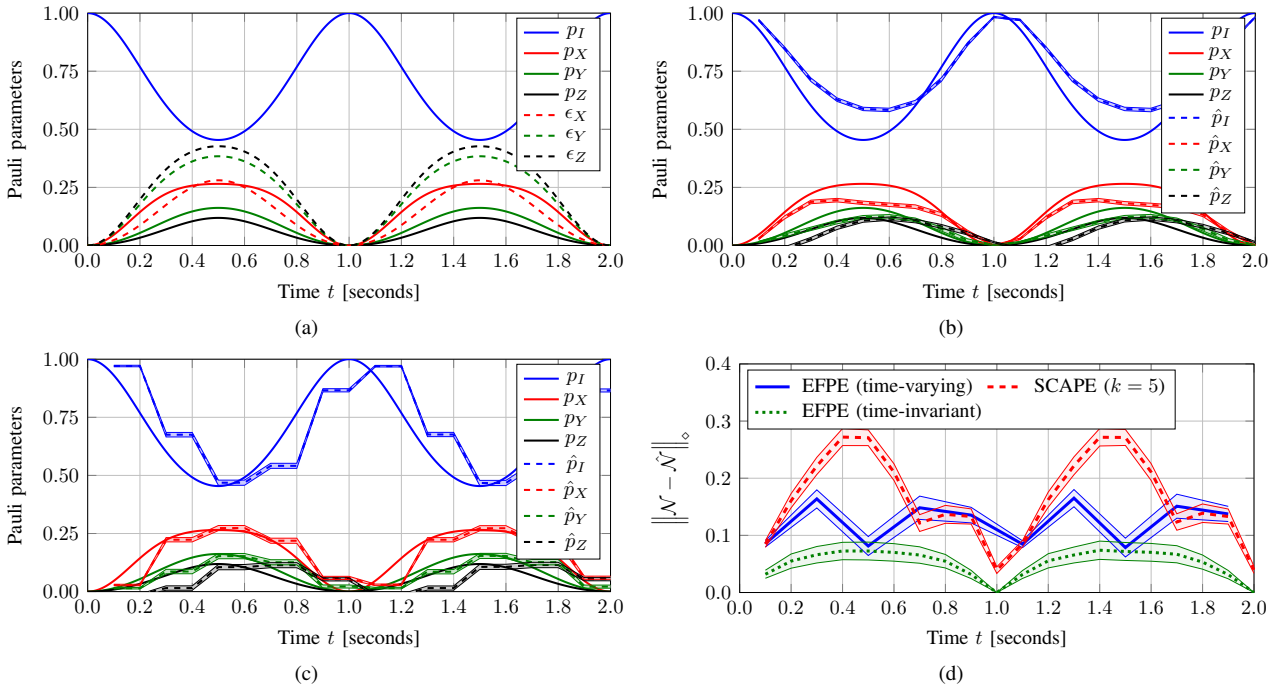

Fig. 4. Performance of Pauli channel estimation of time-varying channels. We plot the time-varying channel parameters in (a). Estimation performance are plotted with (b) SCAPE with $k = 5$, (c) EFPE with communication and estimation in alternative time steps. The diamond norm distance is plotted in (d). For comparison, the diamond norm distance of EFPE on a channel that remains fixed during estimation (time-invariant) is also plotted in (d). Variations in the performance of EFPE (time-invariant) at different instances stem from the different learnability of distinct distributions. Simulation parameters are $N = 10^3$, $M = 10^3$, $a = 0.3$, $b = 0.7$, $f_S = 10^4$, $f = 10^0$, and $\phi = \pi/2$. See the main text for descriptions of simulation parameters.

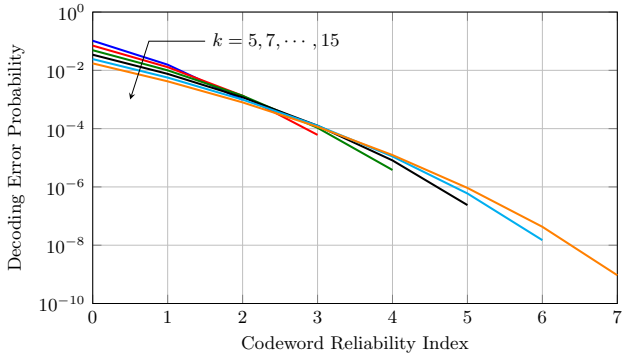

Fig. 5. Decoding error probability (17) of a k-repetition codeword as a function of measured CRI after a channel with the bit-flip probability $p = 1/4$.

is less than or equal to $\frac{k-1}{2}$. We define the following quantity as the CRI for repetition codes

$$C = |N_0 - N_1| - \frac{k-1}{2}, \tag{14}$$

where $|\cdot|$ denotes the absolute value. The CRI is the exact number of bits in a received codeword that can be flipped without changing the decoded bit. Intuitively, higher the value of the CRI lower the chance of incorrect decoding. To see this, consider a noisy channel with the bit-flip probability $p < 1/2$. Then, the probability of decoding error such that the CRI is at least s is

$$\mathbb{P}\left\{\text{Decoding Error} \mid C \geq s\right\} \tag{15}$$

$$= \mathbb{P}\left\{n_f \geq \frac{k+1}{2} + s\right\} \tag{16}$$

$$= \sum_{i=\frac{k+1}{2}+s}^{k} \binom{k}{i} p^i (1-p)^{k-i}, \tag{17}$$

where n_f is the number of bits flipped in a codeword and

$$\binom{k}{i} = \frac{k!}{i!\,(k-i)!} \tag{18}$$

are the binomial coefficients. The decoding error probability decreases for higher values of observed CRI as it removes terms from summation (17). Fig. 5 shows the sharp decreases in the probability of decoding error with increasing values of observed CRI.

After receiving a channel corrupted codeword, receiver decodes the encoded bit by majority voting and also calculates the CRI of the received codeword. If the CRI C of the received codeword is smaller than a predefined threshold $s_{\min}$, the receiver considers the decoded bit as unreliable. If this event occurs frequently, the receiver considers the strength of the employed code insufficient and sends a feedback to the sender to lower the code rate, i.e., to increase k. If the CRI is frequently greater than another predetermined threshold $s_{\max}$, the receiver considers the current code rate to be lower than what is required and sends the feedback to the sender to increase the code rate. Finally, if $s_{\min} \leq C \leq s_{\max}$, the receiver continues with the currently employed code rate.

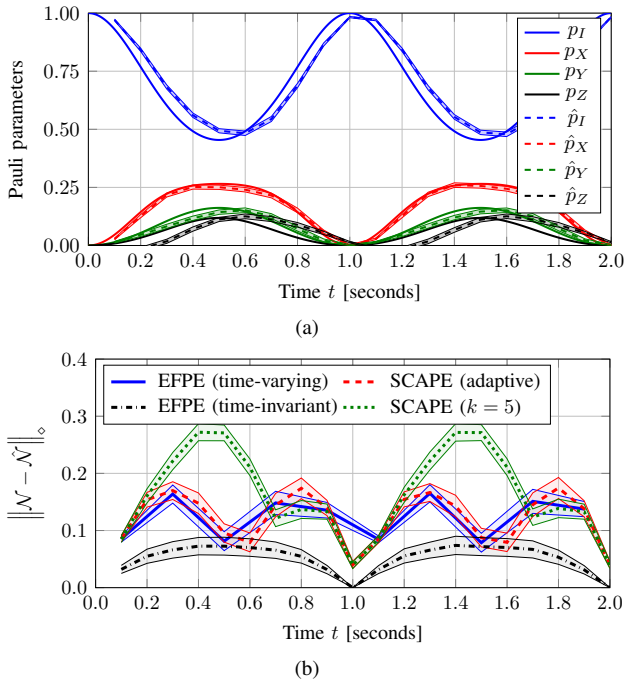

Fig. 6. Estimation performance of SCAPE with adaptive coding rate based on CRI. The tracking of Pauli parameters is plotted in (a). The comparison of obtained performance (diamond norm distance) with different strategies is plotted in (b). Shaded regions show one standard deviation. Adaptive SCAPE performs as good as EFPE while utilizing all channel uses for communication. Here, we have used $s_{\min} = 1$ and $s_{\max} = 3$. Other simulation parameters are $N = 10^3$, $M = 10^3$, $a = 0.3$, $b = 0.7$, $f_S = 10^4$, $f = 10^0$, and $\phi = \pi/2$.

Increasing k improves the probability that the measured value C of CRI is at least $s_{\min}$. For large values of k, this probability approaches unity as shown below.

$$\mathbb{P}\{C \geq s_{\min}\} \tag{19}$$

$$= 1 - \mathbb{P}\left\{\frac{k+1}{2} - s_{\min} \leq n_f \leq \frac{k+1}{2} + s_{\min} - 1\right\} \tag{20}$$

$$= 1 - \sum_{j=\frac{k+1}{2}-s_{\min}}^{\frac{k+1}{2}+s_{\min}-1} \binom{k}{j} p^j (1-p)^{k-j}. \tag{21}$$

Note that the *number of terms* in summation in (21) is constant to $2s_{\min}$. We can equally write the index variable $j = \frac{k+1}{2} - s_{\min} + \ell$ for $0 \leq \ell \leq 2s_{\min} - 1$ and change the summation variable to ℓ. Continuing only with the summation term in (21)

$$\sum_{j=\frac{k+1}{2}-s_{\min}}^{\frac{k+1}{2}+s_{\min}-1} \binom{k}{j} p^j (1-p)^{k-j} \tag{22}$$

$$= \sum_{\ell=0}^{2s_{\min}-1} \binom{k}{\frac{k+1}{2} - s_{\min} + \ell} p^{\frac{k+1}{2}-s_{\min}+\ell} (1-p)^{\frac{k-1}{2}+s_{\min}-\ell} \tag{23}$$

$$= \sum_{\ell=0}^{2s_{\min}-1} \frac{k! p^{\frac{k+1}{2}-s_{\min}+\ell} (1-p)^{\frac{k-1}{2}+s_{\min}-\ell}}{(\frac{k+1}{2} - s_{\min} + \ell)! (\frac{k-1}{2} + s_{\min} - \ell)!}. \tag{24}$$

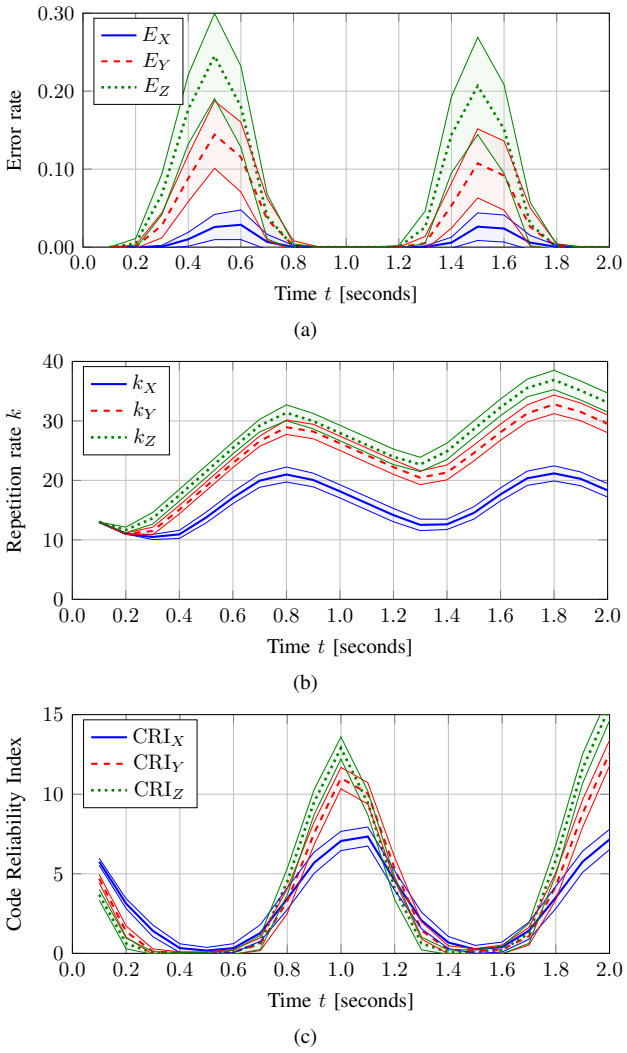

Fig. 7. Communication performance of SCAPE with adaptive coding rate based on CRI. Average bit error rates observed in the message are plotted in (a). The adaptive choices of repetition codes for BSC_X, BSC_Y, and BSC_Z are plotted in (b) denoted as k_X, k_Y, and k_Z, respectively. The CRI for BSC_X, BSC_Y, and BSC_Z are plotted in (c). Shaded regions show one standard deviation. Here, we have used $s_{\min} = 1$ and $s_{\max} = 3$. Other simulation parameters are $N = 10^3$, $M = 10^3$, $a = 0.3$, $b = 0.7$, $f_S = 10^4$, $f = 10^0$, and $\phi = \pi/2$.

Assuming large k, i.e., $k \gg |s_{\min-\ell}|$, we can write

$$(24) \xrightarrow{\text{large } k} (2s_{\min} - 1) \frac{k! p^{k/2} (1-p)^{k/2}}{((k/2)!)^2} \tag{25}$$

$$\overset{(a)}{\approx} (2s_{\min} - 1) (p(1-p))^{k/2} \frac{\sqrt{2\pi k} (k/e)^k}{\left(\sqrt{\pi k} (k/2e)^{k/2}\right)^2} \tag{26}$$

$$= (2s_{\min} - 1) (p(1-p))^{k/2} \frac{2^{k+\frac{1}{2}}}{\sqrt{\pi k}} \tag{27}$$

$$\overset{(b)}{<} \sqrt{\frac{2}{\pi k}} (2s_{\min} - 1), \tag{28}$$

which approaches 0 as $k \to \infty$. Here, approximation (a) is due to the Stirling's approximation of factorial $k! \approx \sqrt{2\pi k} (k/e)^k$ and inequality (b) is obtained since $p(1-p) < 1/4$ for $p <$

$1/2$. Thus, (21) approaches unity for large k. Decreasing the coding rate by increasing k eventually leads to obtaining the CRI above the fixed threshold $s_{\min}$.

Fig. 6 show the estimation performance of this CRI-based adaptive strategy with $s_{\min} = 1$ and $s_{\max} = 3$. The coding rate is changed if a single instance of $s \notin [s_{\min}, s_{\max}]$ in a single estimation step is observed. In Fig. 6(b) we see that this strategy performs as good as EFPE that used separate time intervals for estimation and communication. In Fig. 6(a), we still observe a slight underestimation of channel noise around $t \approx 0.5 \sim 0.6$ and $t \approx 1.5 \sim 1.6$ seconds. This indicates that adaptive choice of k is still not high enough. This observation is complemented by looking at the communication performance of SCAPE.

In Fig. 7, we show the communication performance of SCAPE by plotting the observed error rates, adaptive choices of k, and measured CRI for BSC_X, BSC_Y, and BSC_Z. The communication error rates are plotted in Fig. 7(a), which attain the maximum value of $E_Z \approx 0.25$. These high error rates are the cause of underestimated noise in Fig. 6. From coding rate perspective, these error rates are not surprising since i) we are employing repetition codes, which are known to be inefficient, ii) the highest noise in BSC_Z is $\epsilon_Z = 0.4271$, which is extremely noisy and corresponds to the channel capacity of 0.0154. On the other hand, the highest value of $k_Z = 37$ as observed in Fig. 7(b) corresponds to a code rate $1/k = 0.0270$, almost twice the channel capacity. In terms of our adaptive SCAPE protocol, this means that k has not incremented sufficiently such as to ensure reliable communication. Nevertheless, the receiver is not oblivious to these high error rates and will be alerted due to CRI going to zero as shown in Fig. 7(c). The receiver can reduce the error margin, i.e., increase $s_{\min}$ and $s_{\max}$ to force the higher values of k and reduced error rates.

Thus, CRI-based adaptive strategy is more efficient in terms of channel utilization for communication while still providing accurate estimates of current channel conditions. However, there is still a large performance gap between the channel estimation performance of time-invariant channel and time-varying channel. This gap is due to the second source of error that we discuss below.

B. Sampling Delay

The second source of error in the estimation performance of time-varying channels is the sampling delay. Traditionally, estimation theory deals with an unknown but fixed parameter that needs to be estimated. In fixed parameter estimation, the estimation error decreases by increasing the number of samples. However, for time-varying channels the underlying distribution is continuously changing with time.

Considering a non-zero sampling time $(1/f_S)$ per sample, collecting N samples has time delay of N/f_S. The underlying distribution can change considerably by the time a large number of samples is collected from the channel. An estimate resulting from these samples will already have a large difference with the current channel condition. We call this type of error the sampling delay error. Furthermore, initial samples might

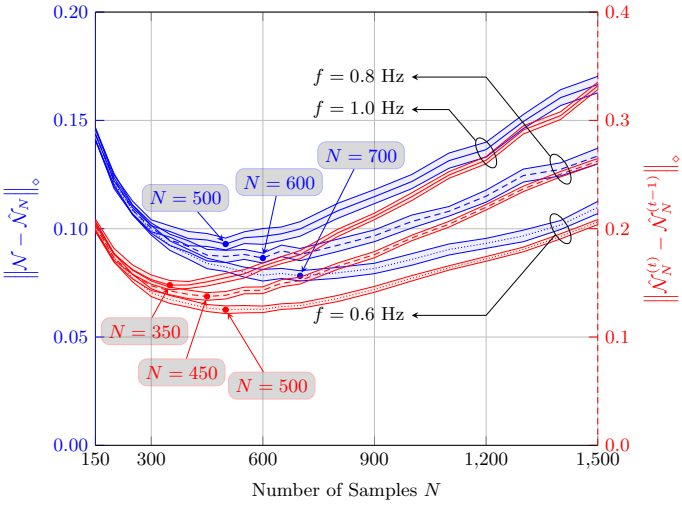

Fig. 8. Visualizing the errors originating by suboptimal N. We plot $\left\|\mathcal{N} - \hat{\mathcal{N}}_N\right\|_\diamond$ (left y-axis, blue plots) and $\left\|\hat{\mathcal{N}}_N^{(t)} - \hat{\mathcal{N}}_N^{(t-1)}\right\|_\diamond$ (right y-axis, red plots) as a function of N for different values of f with adaptive SCAPE. For slowly varying channels, i.e., lower frequencies, it is possible to choose higher values of N to minimize the estimation error or to minimize the inter-estimate fluctuations. Here, we have used $s_{\min} = 1$ and $s_{\max} = 3$. Other simulation parameters are $M = 10^2$, $a = 0.3$, $b = 0.7$, $f_S = 10^4$, and $\phi = \pi/2$.

be originating from an entirely different distribution than the distribution of final samples. An estimate from these samples might not reflect true distribution of any of the collected samples. We call this type of error the distribution varying errors. Note that both sampling delay error and the distribution varying errors can be reduced by decreasing the number of samples N in each estimation step. However, reducing the number of samples can introduce significant statistical errors.

Based on these conflicting types of errors in time-varying quantum channels, we empirically expect the total error $\left\|\mathcal{N} - \hat{\mathcal{N}}_N\right\|_\diamond$ to be a convex function of N achieving its minimum value at some optimal $N = N_{\text{opt}}$, where $\hat{\mathcal{N}}_N$ is the channel estimated over N samples. Sampling delay error and distribution varying errors become dominant for $N > N_{\text{opt}}$. For $N < N_{\text{opt}}$, statistical error is the dominant type of error.

In experimental or simulation situations where the exact channel information is available, it is possible to numerically obtain

$$N_{\text{opt}} = \arg\min_N \left\|\mathcal{N} - \hat{\mathcal{N}}_N\right\|_\diamond \tag{29}$$

by gradient descent. However, $\mathcal{N}$ is not known in practical scenarios (hence the need of channel tomography) and it is not possible to obtain N_{opt} as described above. Another closely related quantity that essentially captures the same notion of sampling delay errors and statistical errors is the relative change between two consecutive channel estimates, i.e., $\left\|\hat{\mathcal{N}}_N^{(t)} - \hat{\mathcal{N}}_N^{(t-1)}\right\|_\diamond$, where $\hat{\mathcal{N}}_N^{(t)}$ is the channel estimate over N samples at time t. This relative change can readily be estimated from already available channel estimates. A high relative change can originate either from N being too large so that the underlying channel has changed significantly or from N being too small introducing significant statistical error

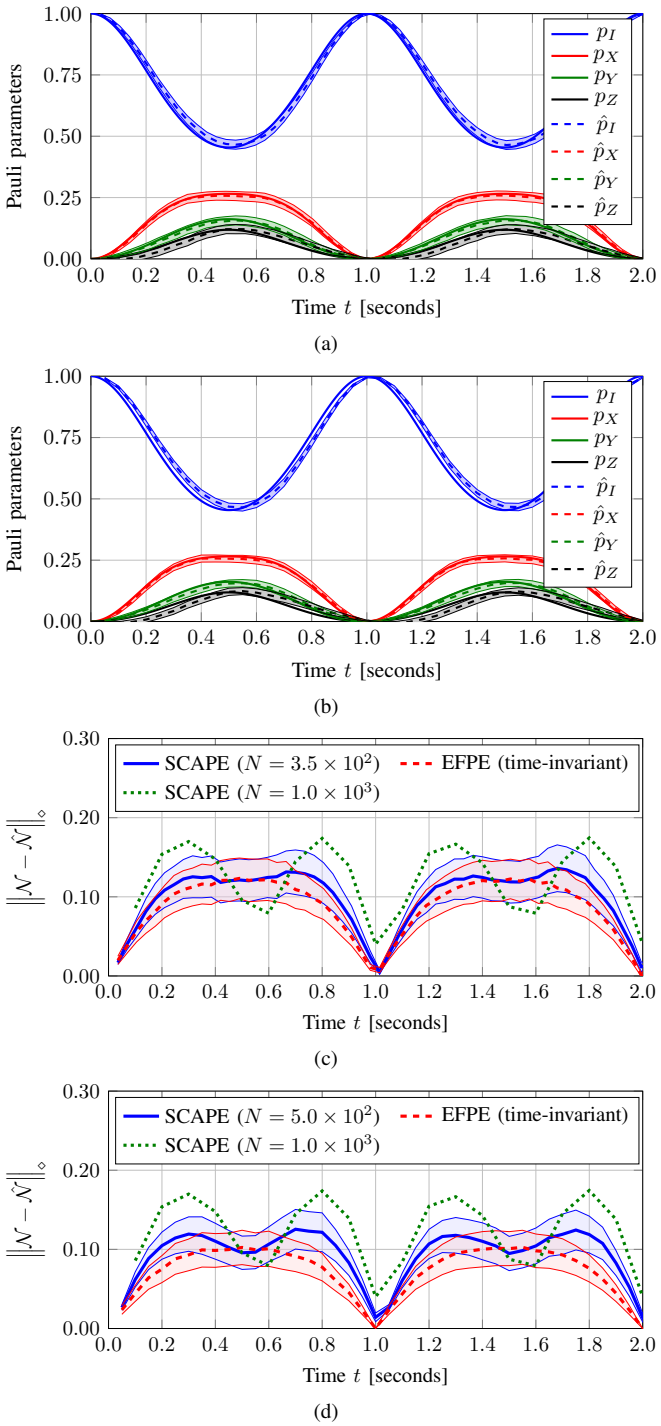

Fig. 9. Estimation performance of adaptive SCAPE with the coding rate based on CRI for (a) $N = 350$ and (b) $N = 500$. The corresponding diamond norm distances are plotted in (c) for $N = 350$ and (d) for $N = 500$. Here, we have used $s_{\min} = 2$ and $s_{\max} = 4$. Other simulation parameters are $M = 10^3$, $a = 0.3$, $b = 0.7$, $f = 10^0$, $f_S = 10^4$, and $\phi = \pi/2$.

appearing in the form of fluctuations in the channel estimates. We empirically expect this quantity to be convex as well based on above arguments.

We plot both of these quantities in Fig. 8 as a function of N for different frequencies f of channel variations. The resulting plots are in agreement with the empirical expectations, i.e., both of these quantities are convex in N and the minimums lie close to each other. As opposed to the update of code rate—which is done after every estimate of the channel—the choice of N can be updated on longer periods. In an estimation scenario with transmitter and receiver, the adaptive SCAPE protocol can be initiated with a large N that sufficiently minimizes the statistical errors. After collecting N_{est} estimates average of $\left\|\hat{\mathcal{N}}_N^{(t)} - \hat{\mathcal{N}}_N^{(t-1)}\right\|_\diamond$ can be calculated over all N_{est} samples. The next N_{est} estimates are obtained over $N - \Delta N$ measurements. This reduction in the number of measurements is continued until the minimum of $\left\|\hat{\mathcal{N}}_N^{(t)} - \hat{\mathcal{N}}_N^{(t-1)}\right\|_\diamond$ is obtained.

In Fig. 9, we plot the estimation performance of SCAPE with adaptive coding rate based on CRI and the number of samples in each estimate as inferred by Fig. 8. We observe that the performance of both $N = 5.0 \times 10^2$ (as obtained by minimizing $\left\|\mathcal{N} - \hat{\mathcal{N}}_N\right\|_\diamond$) and $N = 3.5 \times 10^2$ (by minimizing $\left\|\hat{\mathcal{N}}_N^{(t)} - \hat{\mathcal{N}}_N^{(t-1)}\right\|_\diamond$) is similar. The major difference between the two is between $t \approx 0.4 \sim 0.6$ and $t \approx 1.4 \sim 1.6$, which is actually caused by the sampling delay. During these periods, the channel starts to become less noisy after being maximally noisy. The estimated channel falls between the two points, which coincidently is closer to the instantaneous channel conditions for $N = 500$. The estimation performance in Fig. 9 is not only improved as compared to what we observed in Fig. 6 but also the performance gap between the adaptive SCAPE and EFPE of time-invariant channel is also significantly reduced. Furthermore, the performance of $N = 350$, i.e., Fig. 9(a) is slightly worse that that of $N = 500$, i.e., Fig. 9(b). This was expected since the latter is obtained by minimizing the quantity that we are plotting in Fig. 9. However, in a real-world scenario where the channel knowledge is unavailable, we can achieve suboptimal but still comparable performance of Fig. 9(a) by minimizing an observable convex quantity over several channel uses.

In Fig. 10, we plot the communication performance of adaptive SCAPE for $N = 350$. We have also changed $s_{\min} = 2$ and $s_{\max} = 4$ to improve the communication performance. In Fig. 10(b) and (c), we see higher values of k and CRIs for all three channels. Consequently, we observe in Fig. 10(a) that obtained error rates are lower than what we observed in Fig. 7(a). This results in almost no underestimation of noise observed in Fig. 9(a) and (b). We do not plot these metrics for $N = 500$ because they result in almost exactly the same trends and values, except for CRI_Z which goes as high as 15 at its peak.

V. Summary & Conclusions

We have studied the problem of estimating time-varying Pauli noise. Time-variations in quantum channels introduce additional complexity to an already challenging problem of quantum process tomography. First, if the estimation is performed once at the beginning of a channel utilization round, the obtained estimate might become inaccurate during the channel utilization round since the physical channel would have changed from its initial description. Consequently, the employed ECCs may become inefficient or insufficient to

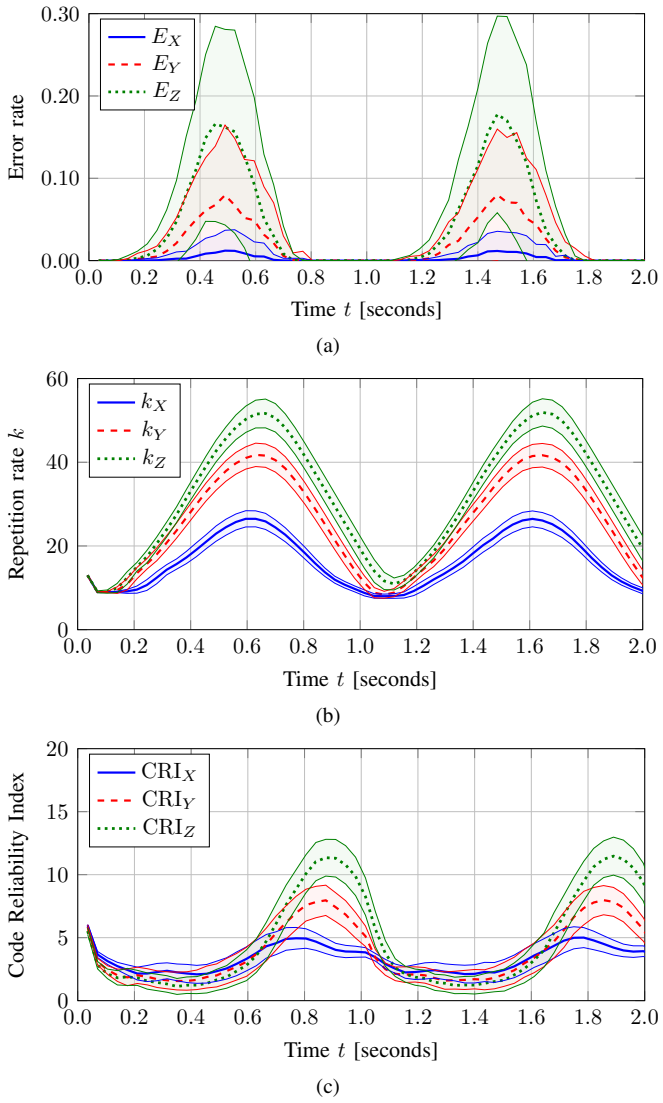

Fig. 10. Communication performance of adaptive SCAPE with the coding rate based on CRI for $N = 350$. We plot the BER on BSC_X, BSC_Y, and BSC_Z in (a), repetition rate k in (b) and obtained CRI values in (c). Here, we have used $s_{\min} = 2$ and $s_{\max} = 4$. Other simulation parameters are $M = 10^3$, $a = 0.3$, $b = 0.7$, $f = 10^0$, $f_S = 10^4$, and $\phi = \pi/2$.

correct encountered channel errors later in the utilization. This necessitates several rounds of channel estimation throughout the channel utilization for up-to-date instantaneous channel estimates. Second, in contrast to the general estimation theory, increasing the number of samples for estimation may have an ill effect of reducing the accuracy of obtained estimates instead of improving it due to sampling delays and change of underlying distribution during the sampling process. This introduces a hard limit on the achievable estimation accuracy and requires non-conventional approaches for choosing optimal number of samples in each estimate. Finally, due to time-variations, the receiver might need to constantly transmit the up-to-date channel description to the transmitter after every estimation round so that the transmitter can decide optimal ECCs. This incurs large amounts of feedback information from receiver to the transmitter.

Adaptive SCAPE appears as a natural candidate for addressing these complex challenges associated with the estimation of time-varying quantum noise. Specially because the communication and channel estimation is performed in the same step. Importantly, the transmitter does not need to know the complete description of the channel. After each step, receiver sends a ternary feedback to the transmitter whether to increase, decrease, or continue with the same rate of ECC. The estimation of optimal number of samples in each estimation round can also be made independently at the receiver's side by computing the relative change of channel estimates, averaged over several round. Interestingly, the inclusion of communication in the estimation does not incur any reduction in the estimation performance as compared to the estimation-only protocols. Finally, the application of adaptive SCAPE goes beyond Pauli noise since arbitrary noise models can be mapped to Pauli noise [10], [26], [30]–[34]. These properties make adaptive SCAPE a natural choice for estimating time-varying quantum noise. Future works may include prediction of channel conditions with machine learning or series forecasting techniques. One particularly interesting experimental direction is the implementation of adaptive SCAPE in practical environments where noise might behave unexpectedly. Implementation of adaptive SCAPE for some more efficient and complex error correcting codes can be an interesting theoretical future work.

REFERENCES

[1] J. Preskill, "Quantum computing in the NISQ era and beyond," *Quantum*, vol. 2, p. 79, Aug. 2018.

[2] M. Kjaergaard, M. E. Schwartz, J. Braumüller, P. Krantz, J. I.-J. Wang, S. Gustavsson, and W. D. Oliver, "Superconducting qubits: Current state of play," *Annu. Rev. Condens. Matter Phys.*, vol. 11, no. 1, pp. 369–395, Mar. 2020.

[3] V. M. Schäfer, C. J. Ballance, K. Thirumalai, L. J. Stephenson, T. G. Ballance, A. M. Steane, and D. M. Lucas, "Fast quantum logic gates with trapped-ion qubits," *Nature*, vol. 555, no. 7694, pp. 75–78, Mar. 2018.

[4] J. M. Lukens and P. Lougovski, "Frequency-encoded photonic qubits for scalable quantum information processing," *Optica*, vol. 4, no. 1, pp. 8–16, Jan 2017.

[5] D. Suter and G. A. Álvarez, "Colloquium: Protecting quantum information against environmental noise," *Rev. Mod. Phys.*, vol. 88, p. 041001, Oct 2016.

[6] Z. Cai, R. Babbush, S. C. Benjamin, S. Endo, W. J. Huggins, Y. Li, J. R. McClean, and T. E. O'Brien, "Quantum error mitigation," *arXiv:2210.00921*, Jun. 2023.

[7] I. L. Chuang and M. A. Nielsen, "Prescription for experimental determination of the dynamics of a quantum black box," *J. Mod. Opt.*, vol. 44, no. 11-12, pp. 2455–2467, Nov. 1997.

[8] Z. Ji, G. Wang, R. Duan, Y. Feng, and M. Ying, "Parameter estimation of quantum channels," *IEEE Trans. Inf. Theory*, vol. 54, no. 11, pp. 5172–5185, Nov. 2008.

[9] A. Fujiwara, "Estimation of a generalized amplitude-damping channel," *Phys. Rev. A*, vol. 70, no. 1, p. 8, Jul. 2004.

[10] R. Harper, S. T. Flammia, and J. J. Wallman, "Efficient learning of quantum noise," *Nat. Phys.*, vol. 16, no. 12, pp. 1184–1188, Dec. 2020.

[11] Y. Fujiwara, "Instantaneous quantum channel estimation during quantum information processing," *arXiv:1405.6267 [quant-ph]*, Apr. 2014. [Online]. Available: https://arxiv.org/abs/1405.6267

[12] M.-X. Huo and Y. Li, "Learning time-dependent noise to reduce logical errors: real time error rate estimation in quantum error correction," *New J. Phys.*, vol. 19, no. 12, p. 123032, Dec. 2017.

[13] T. Wagner, H. Kampermann, D. Bruß, and M. Kliesch, "Optimal noise estimation from syndrome statistics of quantum codes," *Phys. Rev. Research*, vol. 3, p. 013292, Mar 2021.

[14] T. Wagner, H. Kampermann, D. Bruß, and M. Kliesch, "Pauli channels can be estimated from syndrome measurements in quantum error correction," *arXiv:2107.14252 [quant-ph]*, Jul. 2021. [Online]. Available: https://arxiv.org/abs/2107.14252
[15] L. Csató and M. Opper, "Sparse on-line Gaussian processes," *Neural Comput.*, vol. 14, no. 3, pp. 641–668, Mar. 2002.
[16] J. ur Rehman and H. Shin, "Simultaneous communication and parameter estimation of pauli channels," in *ICC 2022 - IEEE International Conference on Communications*, Seoul, South Korea, May 2022, pp. 648–653.
[17] P. V. Klimov, J. Kelly, Z. Chen, M. Neeley, A. Megrant, B. Burkett, R. Barends, K. Arya, B. Chiaro, Y. Chen, A. Dunsworth, A. Fowler, B. Foxen, C. Gidney, M. Giustina, R. Graff, T. Huang, E. Jeffrey, E. Lucero, J. Y. Mutus, O. Naaman, C. Neill, C. Quintana, P. Roushan, D. Sank, A. Vainsencher, J. Wenner, T. C. White, S. Boixo, R. Babbush, V. N. Smelyanskiy, H. Neven, and J. M. Martinis, "Fluctuations of energy-relaxation times in superconducting qubits," *Phys. Rev. Lett.*, vol. 121, p. 090502, Aug 2018.
[18] J. J. Burnett, A. Bengtsson, M. Scigliuzzo, D. Niepce, M. Kudra, P. Delsing, and J. Bylander, "Decoherence benchmarking of superconducting qubits," *npj Quantum Inform.*, vol. 5, no. 1, Jun. 2019.
[19] J. Etxezarreta Martinez, P. Fuentes, P. Crespo, and J. Garcia-Frias, "Time-varying quantum channel models for superconducting qubits," *npj Quantum Inform.*, vol. 7, no. 1, pp. 1–10, Jul. 2021.
[20] S. Pirandola, "Satellite quantum communications: Fundamental bounds and practical security," *Phys. Rev. Res.*, vol. 3, p. 023130, May 2021.
[21] J. Etxezarreta Martinez, P. Fuentes, A. deMarti iOlius, J. Garcia-Frías, J. R. Fonollosa, and P. M. Crespo, "Multi-qubit time-varying quantum channels for NISQ-era superconducting quantum processors," *arXiv:2207.06838*, Sep. 2022.
[22] Y. Hirasaki, S. Daimon, T. Itoko, N. Kanazawa, and E. Saitoh, "Detection of temporal fluctuation in superconducting qubits for quantum error mitigation," *arXiv:2307.04337*, Jul. 2023.
[23] J. ur Rehman and H. Shin, "Entanglement-free parameter estimation of generalized Pauli channels," *Quantum*, vol. 5, p. 490, Jul. 2021.
[24] J. ur Rehman, Y. Jeong, J. S. Kim, and H. Shin, "Holevo capacity of discrete Weyl channels," *Sci. Rep.*, vol. 8, no. 1, p. 17457, Nov. 2018.
[25] H. Shin and M. Z. Win, "MIMO diversity in the presence of double scattering," *IEEE Trans. Inf. Theory*, vol. 54, no. 7, pp. 2976–2996, Jul. 2008.
[26] J. J. Wallman and J. Emerson, "Noise tailoring for scalable quantum computation via randomized compiling," *Phys. Rev. A*, vol. 94, p. 052325, Nov. 2016.
[27] A. Y. Kitaev, "Quantum computations: Algorithms and error correction," *Russ. Math. Surv.*, vol. 52, no. 6, pp. 1191–1249, Dec. 1997.
[28] G. Benenti and G. Strini, "Computing the distance between quantum channels: Usefulness of the Fano representation," *J. Phys. B-At. Mol. Opt. Phys.*, vol. 43, no. 21, p. 215508, Oct. 2010.
[29] M. F. Sacchi, "Optimal discrimination of quantum operations," *Phys. Rev. A*, vol. 71, no. 6, p. 4, Jun. 2005.
[30] Z. Puchała, Ł. Rudnicki, and K. Życzkowski, "Pauli semigroups and unistochastic quantum channels," *Phys. Lett. A*, vol. 383, no. 20, pp. 2376–2381, Jul. 2019.
[31] E. Knill, "Quantum computing with realistically noisy devices," *Nature*, vol. 434, no. 7029, pp. 39–44, Mar. 2005.
[32] J. Emerson, M. Silva, O. Moussa, C. Ryan, M. Laforest, J. Baugh, D. G. Cory, and R. Laflamme, "Symmetrized characterization of noisy quantum processes," *Science*, vol. 317, no. 5846, pp. 1893–1896, Sep. 2007.
[33] M. R. Geller and Z. Zhou, "Efficient error models for fault-tolerant architectures and the Pauli twirling approximation," *Phys. Rev. A*, vol. 88, p. 012314, Jul. 2013.
[34] Z. Cai, X. Xu, and S. C. Benjamin, "Mitigating coherent noise using Pauli conjugation," *npj Quantum Inform.*, vol. 6, no. 1, p. 17, Feb. 2020.

Junaid ur Rehman received the B.S. degree in Electrical Engineering from National University of Sciences and Technology (NUST), Islamabad, Pakistan, in 2013, and the Ph.D. degree in Electronic Engineering from Kyung Hee University (KHU), Yongin-si, Korea, in 2019.

He worked as a Postdoctoral Fellow at KHU (2019-2020) and Korea Institute of Science and Technology (KIST) (2020). Later he joined KHU as a Research Professor from 2021-2022. In 2022, he joined the Interdisciplinary Centre for Security, Reliability and Trust (SnT), University of Luxembourg where he is currently a Research Scientist in the Signal Processing and Communications (SigCom) group. His research interests include quantum information sciences that include quantum communications, quantum computing, and quantum sensing.

Dr. ur Rehman has served as a technical program committee member of multiple IEEE conferences including IEEE International Conference on Communications (ICC) and IEEE Global Communications Conference (Globecom). He has reviewed for numerous IEEE conferences and journals. He was an Exemplary Reviewer for the IEEE WIRELESS COMMUNICATIONS LETTERS in 2022.

Hayder Al-Hraishawi (S'13-M'17-SM'23) received the Ph.D. degree from the Department of Electrical and Computer Engineering, Southern Illinois University Carbondale, USA, in 2017. Currently, he is a Research Scientist at the Interdisciplinary Centre for Security, Reliability and Trust (SnT), University of Luxembourg. He also has a strong engineering professional with over five years of experience in industry and leadership roles gained from holding various positions at prestigious telecom companies such as Motorola Solutions, Huawei Technologies, and Nokia Networks. He is a member (Associate Editor) in the editorial board of IEEE Access journal since 2019. He was an Exemplary Reviewer for the IEEE Transaction on Communications (TCOM) in 2022. He has served as a member of Technical Program Committee (TPC) for several IEEE conferences, including ICC, GLOBECOM, and WCNC. His research interests span the broad areas of terrestrial and non-terrestrial communications networks and signal processing including spectrum-sharing and resource allocation techniques for massive MIMO systems, reconfigurable intelligent surfaces, and satellite communication systems.

Trung Q. Duong (Fellow, IEEE) is a Canada Excellence Research Chair (CERC) and a Full Professor at Memorial University of Newfoundland, Canada and is also the Chair Professor in Telecommunications at Queen's University Belfast, UK. He has received the two prestigious Research Chair of the Royal Academy of Engineering (2021-2025) and the Royal Academy of Engineering Research Fellowship (2015-2020). He was a Distinguished Advisory Professor at Inje University, South Korea (2017-2019). He is an Adjunct Professor and the Director of Institute for AI and Big Data at Duy Tan University, Vietnam (2012-present), a Distinguished Professor at Thuyloi University, Vietnam (2023-2028) and a Visiting Professor (under Eminent Scholar program) at Kyung Hee University, South Korea (2023-2024). His current research interests include quantum communications, wireless communications, signal processing, machine learning, and realtime optimisation.

Dr. Duong has served as an Editor/Guest Editor for the IEEE TRANSACTIONS ON WIRELESS COMMUNICATIONS, IEEE TRANSACTIONS ON COMMUNICATIONS, IEEE TRANSACTIONS ON VEHICULAR TECHNOLOGY, IEEE COMMUNICATIONS LETTERS, IEEE WIRELESS COMMUNICATIONS LETTERS, IEEE WIRELESS COMMUNICATIONS, IEEE COMMUNICATIONS MAGAZINES, and IEEE JOURNAL ON SELECTED AREAS IN COMMUNICATIONS. He received the Best Paper Award at the IEEE VTC-Spring 2013, IEEE ICC 2014, IEEE GLOBECOM 2016, 2019, 2022, IEEE DSP 2017, IWCMC 2019, 2023, and IEEE CAMAD 2023. He is the recipient of the prestigious Newton Prize 2017. He is a Fellow of Asia-Pacific Artificial Intelligence Association (AAIA).

Symeon Chatzinotas (Fellow, IEEE) is currently Full Professor / Chief Scientist I and Head of the research group SIGCOM in the Interdisciplinary Centre for Security, Reliability and Trust, University of Luxembourg. In parallel, he is an Adjunct Professor in the Department of Electronic Systems, Norwegian University of Science and Technology and a Collaborating Scholar of the Institute of Informatics & Telecommunications, National Center for Scientific Research "Demokritos". In the past, he has lectured as Visiting Professor at the University of Parma, Italy and contributed in numerous R&D projects for the Institute of Telematics and Informatics, Center of Research and Technology Hellas and Mobile Communications Research Group, Center of Communication Systems Research, University of Surrey.

He was the co-recipient of the 2014 IEEE Distinguished Contributions to Satellite Communications Award and Best Paper Awards at EURASIP JWCN, CROWNCOM, ICSSC. He has (co-)authored more than 500 technical papers in refereed international journals, conferences and scientific books.

Hyundong Shin (Fellow, IEEE) received the B.S. degree in Electronics Engineering from Kyung Hee University (KHU), Yongin-si, Korea, in 1999, and the M.S. and Ph.D. degrees in Electrical Engineering from Seoul National University, Seoul, Korea, in 2001 and 2004, respectively. During his postdoctoral research at the Massachusetts Institute of Technology (MIT) from 2004 to 2006, he was with the Laboratory for Information Decision Systems (LIDS). In 2006, he joined the KHU, where he is currently a Professor in the Department of Electronic Engineering. His research interests include quantum information science, wireless communication, and machine intelligence. Dr. Shin received the IEEE Communications Society's Guglielmo Marconi Prize Paper Award and William R. Bennett Prize Paper Award. He served as the Publicity Co-Chair for the IEEE PIMRC and the Technical Program Co-Chair for the IEEE WCNC and the IEEE GLOBECOM. He was an Editor of IEEE TRANSACTIONS ON WIRELESS COMMUNICATIONS and IEEE COMMUNICATIONS LETTERS.